Dalton Transactions

Accepted Manuscript

This article can be cited before page numbers have been issued, to do this please use: O. V. Yakubovich, G. Kiriukhina, O. Dimitrova, E. A. Zvereva, L. V. Shvanskaya, O. S. Volkova and A. N. Vasiliev, *Dalton Trans.*, 2015, DOI: 10.1039/C5DT04543F.

This is an *Accepted Manuscript*, which has been through the Royal Society of Chemistry peer review process and has been accepted for publication.

Accepted Manuscripts are published online shortly after acceptance, before technical editing, formatting and proof reading. Using this free service, authors can make their results available to the community, in citable form, before we publish the edited article. We will replace this *Accepted Manuscript* with the edited and formatted *Advance Article* as soon as it is available.

You can find more information about *Accepted Manuscripts* in the Information for Authors.

Please note that technical editing may introduce minor changes to the text and/or graphics, which may alter content. The journal's standard Terms & Conditions and the Ethical guidelines still apply. In no event shall the Royal Society of Chemistry be held responsible for any errors or omissions in this *Accepted Manuscript* or any consequences arising from the use of any information it contains.

ROYAL SOCIETY OF CHEMISTRY

www.rsc.org/dalton

ROYAL SOCIETY OF CHEMISTRY View Article Online
DOI: 10.1039/C5DT04543F

Journal Name

ARTICLE

An open framework crystal structure and physical properties of $RbCuAl(PO_4)_2$

Received 00th January 20xx,
Accepted 00th January 20xx

DOI: 10.1039/x0xx00000x

www.rsc.org/

Olga V. Yakubovich,[a] Galina V. Kiriukhina,[a] Olga V. Dimitrova,[a] Elena A. Zvereva,[a] Larisa V. Shvanskaya,[a,b] Olga S. Volkova[a,b,c] and Alexander N.Vasiliev[a,b,c]

The novel phosphate $RbCuAl(PO_4)_2$ was prepared by hydrothermal synthesis at 553K. Its crystal structure was determined using single-crystal X-ray diffraction data and refined against F^2 to R = 0.026. The compound crystallizes in the monoclinic space group $P2_1/c$, with unit-cell parameters a = 5.0723(8) Å, b = 14.070(2) Å, c = 9.352(1) Å, β = 100.41(1), V = 656.4(2) Å^3, and Z = 4. The crystal structure is based on an open 3*D* aluminophosphate framework built by AlO_5 bipyramids and PO_4 tetrahedra sharing oxygen vertices. Channels in the [100] and [001] directions accommodate Rb^+ cations and chains of Cu-centered octahedra alternatively sharing *cis*- and *trans*- edges. The new phase is characterized by the structure type established for isotypic iron phosphates $KMFe(PO_4)_2$, where *M* = Fe/Ni, Ni, Mg or Co. It also shows topological relationships with $Pb_2Ni(PO_4)_2$ and $Fe^{3+}Fe^{2+}_{0.5}(H_2O)_2(HPO_4)_2$ structures. The $RbCuAl(PO_4)_2$ exhibits rather peculiar physical properties evidenced in specific heat and magnetization measurements. It releases a significant part of magnetic entropy well above the Neel temperature T_N = 10.5 K and possesses spontaneous magnetic moment at lower temperatures. The origin of the spontaneous moment is ascribed to the canting of a pristine antiferromagnetic structure due to the interchain Dzyaloshinskii – Moriya exchange interaction.

Introduction

Many transition metal phosphates serve as basis of functional materials for different technologies. They are extensively investigated as high power cathode materials for rechargeable low cost and environmentally friendly lithium- and sodium-ion batteries, as oxygen evolution catalysts in solar fuel production devices, as pigments because of high anticorrosion properties, as non-linear optical materials, and molecular sieves.[1-4] They frequently present multifunctional materials based on open-network structures built from different kind of acid and amphoteric oxo-complexes. Thus, aluminophosphate zeotype compounds with different crystal structures built from oxo-tetrahedra and MO_n (n = 3–6) metal-centered polyhedra are characterized by high thermal and chemical stability and potentially enhanced functionality.[5] Transition metal (alumino)phosphates with porous framework crystal structures often combine zeolite-like and magnetic properties.[6] Most among them are iron-based phases, although several examples of cobalt, manganese, nickel and copper (alumino)phosphates have been cited in the last years. All these compounds with porous 3*D*-frameworks usually show various types of magnetic interactions between transition metal centres: the magnetic exchange interactions can be realized through oxygen bridges, alternatively the superexchange interactions may occur by means of phosphate and alumina side groups.

In our search for functional crystals with mixed anionic framework arrangement a novel rubidium copper aluminophosphate was obtained under hydrothermal conditions. We present here its open-framework crystal structure in comparison with related Ni- and Fe-phosphates of similar topologies and physical properties.

Experimental procedure

Blue crystals of the new phase with a maximum lengthening of 500 μm (Fig. 1) were grown under hydrothermal conditions in the $RbNO_3$–CuO–$AlPO_4$ system. A mixture of the essential components in the 1:1:1 weight ratio was placed in a 5ml. stainless steel bomb with distilled water filling 80% of the volume. A small amount of H_3BO_3 (5 wt.%) was added to the starting materials as a mineralizer. The experiment was conducted at a temperature of 553 K and a pressure of 70 bars over a period of 18 days. The reaction products were the new phase in an amount estimated of 40 % of the total yield, light blue crystals of $Cu_3(PO_4)_2$ (a triclinic modification) and uncolored prismatic crystals of synthetic berlinite, $AlPO_4$. After cooling of the furnace the crystals were separated by filtration,

[a] M.V. Lomonosov Moscow State University, Moscow 119991, Russia. E-mail: yakubol@geol.msu.ru
[b] National University of Science and Technology "MISiS", Moscow 119049, Russia.
[c] Ural Federal University, Ekaterinburg 620002, Russia.

Electronic Supplementary Information (ESI) available: crystallographic information file (cif-file) for $RbCuAl(PO_4)_2$ compound, atomic coordinates and equivalent isotropic displacement parameters, bond-valence data. See DOI: 10.1039/x0xx00000x

View Article Online
DOI: 10.1039/C5DT04543F

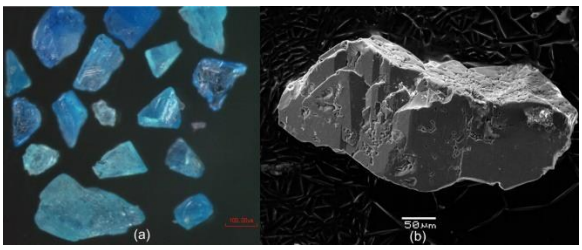

Fig. 1 Photo of crystals of the title compound (a) and SEM image, showing the crystal morphology (b).

washed with water, dried and analyzed with a scanning electron microscope (SEM)[‡]. The JEOL SEM (JSM-6480LV) was equipped with an INCA Energy-350 energy dispersive (EDS) detector and an INCAWave-500 four-crystal wavelength dispersive (WDS) spectrometer. The measurements were made at 20 kV and 7 nA for which the sample was stable. The following standards were used: CuO (Cu), $AlPO_4$ (Al & P), $Rb_2Nb_4O_{11}$ (Rb). X-ray spectral analysis of a polished sample showed a semi quantitative Rb:Cu:P:Al ration equal to 1:1:2:1, which is fully consistent with the results of our X-ray diffraction structural study.

The single crystal X-ray diffraction data were collected at an Xcalibur-S area detector diffractometer using MoK_α radiation (graphite monochromator). The intensities were corrected for Lorentz and polarization effects, and a numerical absorption correction based on Gaussian integration over a multifaceted crystal model was applied. The crystallographic characteristics of the new phase, the experimental conditions of data collection and final results of structure refinement are shown in Table 1. All of the calculations were performed in a framework of the WinGX32 software package.[7] Atomic scattering factors and anomalous dispersion corrections were taken from the International Tables for Crystallography.[8] The crystal structure was solved via direct methods in the space group $P2_1/c$ using the SIR-92 program[9] and refined against the F^2 data with SHELXL10 to the final R factor of 0.026 (for 1392 unique reflections with I > 2σ(I)), using anisotropic displacement parameters. Characteristic distances are given in Table 2. A bond-valence calculation (Table S2) has been performed using the algorithm and parameters offered in[11, 12]; its results are consistent with the assumed oxidation state of Cu. The synthesized phase is characterized by the following chemical formula: $RbCuAl(PO_4)_2$[§].

Results and discussion

Description of the crystal structure. The asymmetric unit of the structure (Fig. 2) includes two P sites in tetrahedral coordination. Three resembling in size P1–O distances of about 1.53 Å and a longer one of 1.567(2) Å characterize the $P1O_4$ polyhedron. On the contrary, there is one relatively short P2–O1 bond length of 1.514(3) Å, two equal bonds of 1.533 Å and one somewhat longer P2–O6 bond length of 1.547(2) Å in the $P2O_4$ tetrahedron. Copper atoms show strongly distorted octahedral coordination in accordance with the Jahn-Teller effect of the d[9]

Table 1 Crystal information and details of the X-ray data collection and refinement

Crystal data	
Chemical formula, M (g mol^{-1})	$RbCuAl(PO_4)_2$, 365.93
Crystal. system, Space group	monoclinic, $P2_1/c$ (no. 14)
a, b, c (Å), β (°)	5.0723(8), 14.070(2), 9.3520(10), 100.410(10)
V (Å^3), Z	656.44(16), 4
D_c (g cm^{-3})	3.703
Crystal size (mm)	0.087 × 0.118 × 0.124
Crystal colour	blue
Absorption coeff. μ(mm^{-1})	11.327
Data collection	
Diffractometer	Xcalibur-S, CCD
Radiation	Mo-K_α (λ = 0.71073 Å), graphite monochromator
Temperature (K)	293(2)
Scanning mode	ω
Measuring range	$2\vartheta_{max}$ = 55.0°
Reflections (total)	10519
R_{int}, $R(\sigma)$	0.0516, 0.0304
h, k, l range	$-6 \le h \le 6$, $-18 \le k \le 18$, $-12 \le l \le 12$
Refinement	
Reflections unique/observed ($I > 2\sigma(I)$)	1512, 1394
Number of parameters used in the ref.	119
Absorption correction, T_{max}, T_{min}	numerical, 0.291, 0.477
Extinction coefficient	0.0010(3)
Residuals	
R (observed reflections)	0.0264
R, w R_2 (all reflections)	0.0303, 0.0593
Goodness of fit S	1.137
δρ (max/min) (e Å^{-3})	0.687, -0.812

Table 2 Interatomic Distances (Å)

Cu octahedron		Rb 12-vertex polyhedron			
Cu – O3	1.921(2)	Rb1 –O8	2.945(3)	Rb1 –O5	3.106(2)
O5	1.975(2)	O3	2.992(2)	O1	3.185(3)
O7	1.984(2)	O7	3.009(3)	O4	3.326(2)
O7	1.989(2)	O2	3.050(3)	O3	3.362(3)
O6	2.443(2)	O4	3.056(2)	O6	3.376(3)
O5	2.507(2)	O1	3.099(3)	O8	3.419(2)
P1 tetrahedron		**P2 tetrahedron**		**Al bipyramid**	
P1 – O4	1.524(3)	P2 –O1	1.514(3)	Al –O6	1.792(3)
O3	1.529(3)	O5	1.533(3)	O2	1.793(3)
O8	1.532(2)	O2	1.533(2)	O8	1.800(3)
O7	1.567(2)	O6	1.547(2)	O4	1.893(3)
				O1	1.905(3)

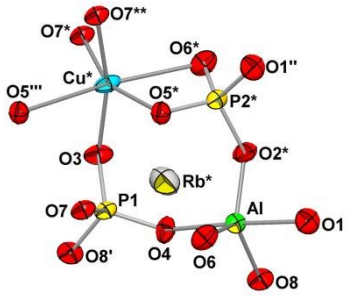

Fig. 2 Basic structural units with atom labeling scheme. Displacement ellipsoids are presented at the 90% probability level. Symmetry codes: (*) –1+x, y, z; (**) 1–x, 1–y, 2–z; (') x, ½–y, ½+z; ('') 1–x, 1–y, 1–z ; (''') 2–x, 1–y, 2–z.

configuration. They are characterized by a square with four Cu–O distances ranging between 1.921(2) and 1.989(2) Å and two elongated bonds in a *trans*-position equal to 2.443(2) and 2.507(2) Å. The Al atoms are surrounded by O atoms, forming five-vertex polyhedra with Al–O bond lengths in the interval 1.793(3) –1.905(3) Å (Table 2). The patterns of distortion of the P-, Cu- and Al-polyhedra are consistent with the bond-valence calculation (Table S2). The Rb^+ cations have eight Rb–O distances varying from 2.945(2) to 3.186(3) Å and four longer ones ranging from 3.326(2) and 3.419(2) Å (Fig. 3). Alternating along [100] direction Cu atoms form corrugated chains of edge-sharing CuO_6 octahedra (Figure 4). The $P2O_4$ tetrahedra share one edge with Cu-centered octahedra, while the $P1O_4$ tetrahedra share two O vertices with neighboring along the chain copper polyhedra with the formation of festoons of the $[Cu(PO_4)_2]_\infty$ composition. These garlands built from Cu- and P-centered polyhedra are cross-linked by AlO_5 bipyramids in a three-dimensional framework with open channels parallel to the *a* and *c* axis of the unit-cell, where the large Rb^+ ions are distributed. These channels are rimed by six-membered rings built from one CuO_6 octahedron, two AlO_5 bipyramids, and three PO_4 tetrahedra (Fig. 5). The new compound is isotypic with the K(Ni,Fe)Fe$(PO_4)_2$ phase and three recently published iron phosphates K*M*Fe$(PO_4)_2$, where *M* = Ni, Mg or Co, all synthesized using the flux method.[13,14] However, the bond lengths in the Cu-octahedra and Al-bipyramids differ significantly from the interatomic distances in corresponding

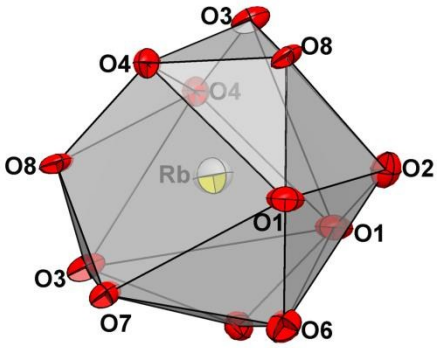

Fig. 3 Coordination polyhedron of Rb (CN 12).

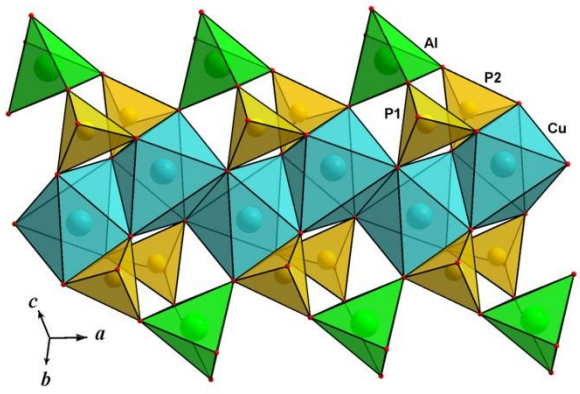

Fig 4 Corrugated chains of CuO_6 octahedra sharing edges, associated with PO_4 tetrahedra and AlO_5 polyhedra.

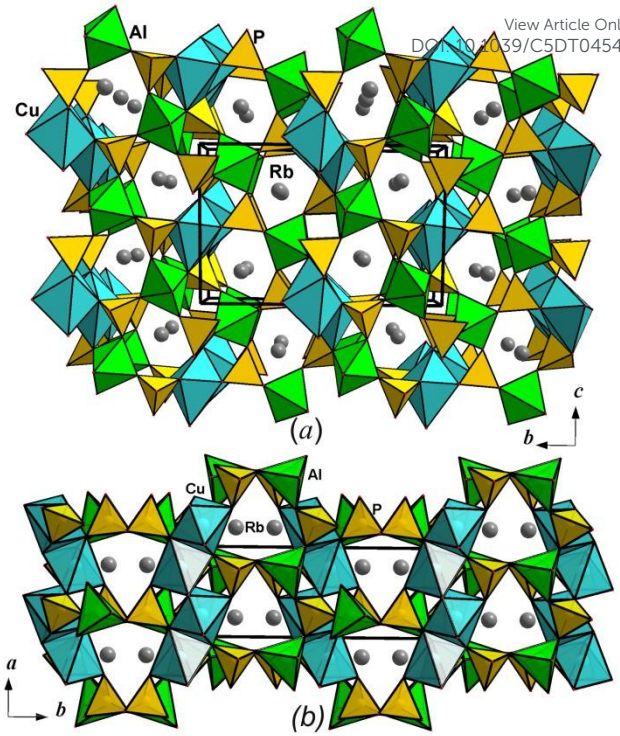

Fig. 5 The title crystal structure in an axonometric projection: viewed along a axis (a) and c axis (b).

polyhedra in the K*M*Fe$(PO_4)_2$ structures. Thus, the CuO_6 octahedra with four Cu–O distances in the square ranging between 1.921(2) and 1.989(2) Å and two elongated bonds in the *trans*-position equal to 2.443(2) and 2.507(2) Å are much stronger distorted compared to the MO_6 (*M* = Ni/Fe, Ni, Mg or Co) polyhedra in the K*M*Fe$(PO_4)_2$ structures, where *M*–O distances lie in the interval 2.01–2.30 Å (Table 3). In the five-vertex Al polyhedral, Al–O bond lengths in the interval 1.793(3) –1.905(3) Å are considerably smaller then likened Fe–O distances in the K*M*Fe$(PO_4)_2$ structures. It should be noted here that no investigation of magnetic properties and specific heat measuring were undertaken for these compounds.

The RbCuAl$(PO_4)_2$ structure may be also treated as formed by aluminophosphate chains of AlO_5 and PO_4 polyhedra sharing oxygen vertices. The chains extending along the crystallographic [100] direction are built from centrosymmetric four-membered rings consisting of two PO_4 tetrahedra and two AlO_5 bipyramids (Fig. 6). The AlO_5 polyhedra share fifth oxygen vertices with additional PO_4 tetrahedra to form a 3*D* $[Al(PO_4)_2]^{3-}_\infty$ para-framework with pendant (not shared with AlO_5 polyhedra) O3 and O7 vertices of the $P1O_4$ tetrahedra and O5 vertices of the $P2O_4$ tetrahedra (Fig. 7a). The chains of CuO_6 octahedra sharing alternatively *cis*- and *trans*- edges are intruded in an open space between these pendant oxygen vertices (Fig. 5). Topologically similar to the described above $[Al(PO_4)_2]^{3-}_\infty$ three-dimensional framework constructions may be easily distinguished in two synthetic phosphates with transition metals, e.g. $Pb_2Ni(PO_4)_2$[15] and $Fe^{3+}Fe^{2+}_{0.5}(H_2O)_2(HPO_4)_2$.[16] All three monoclinic phases have

View Article Online
DOI: 10.1039/C5DT04543F

Journal Name

ARTICLE

Table 3 Selected bond lengths in the crystal structures of isotypic phosphates $AM^{2+}M^{3+}(PO_4)_2$ (space group $P2_1/c$, Z=4)

Formula	MO_6 octahedron M^{2+}-O range; < M^{2+}-O>, Å	MO_5 polyhedron M^{3+}-O range; < M^{3+}-O>, Å	$P1O_4$ tetrahedron, P-O range; < P-O>, Å	$P2O_4$ tetrahedron, P-O range; < P-O>, Å	Ref.
$K(Ni_{0.93}Fe^{2+}_{0.07})Fe^{3+}(PO_4)_2$	2.014 – 2.198; 2.090	1.892 – 2.017; 1.937	1.522 – 1.567; 1.537	1.521 – 1.556; 1.537	13
$KNiFe^{3+}(PO_4)_2$	2.014 – 2.200; 2.090	1.891 – 2.012; 1.934	1.523 – 1.569; 1.537	1.520 – 1.559; 1.538	14
$KMgFe^{3+}(PO_4)_2$	2.005 – 2.234; 2.105	1.898 – 2.013; 1.939	1.522 – 1.564; 1.536	1.517 – 1.553; 1.537	14
$KCo^{2+}Fe^{3+}(PO_4)_2$	2.007 – 2.298; 2.122	1.892 – 2.001; 1.934	1.518 – 1.566; 1.534	1.518 – 1.552; 1.534	14
$RbCu^{2+}Al(PO_4)_2$	1.921 – 2.507; 2.136	1.792 – 1.905; 1.837	1.524 – 1.567; 1.538	1.514 – 1.547; 1.532	Our data

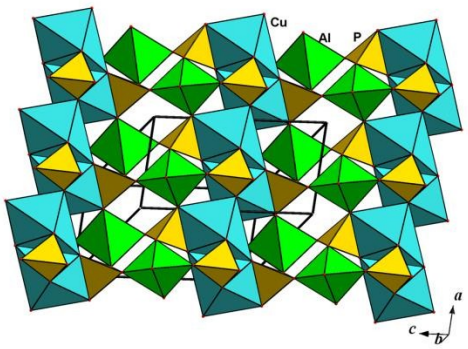

Fig. 6 Aluminophosphate chains built by AlO_5 and PO_4 polyhedra sharing oxygen vertices in the $RbCuAl(PO_4)_2$ structure.

close values of the unit-cell parameters and volumes (Table 4). All 3*D* frameworks are built by alternating phosphate tetrahedra and amphoteric oxo-complexes formed by Al^{3+}, Ni^{2+} or Fe^{3+}/Fe^{2+} ions. Besides different charge of cations they are also characterized by diverse coordination numbers and various coordination polyhedra. Thus, in the $RbCu[Al(PO_4)_2]$, AlO_5 bipyramids and PO_4 tetrahedra sharing vertices, constitute 12-membered rings, which rimed channels running parallel to the [100] direction enclose the Rb and Cu atoms (Figure 7a). Rings of similar shape and topology built from NiO_6 octahedra and PO_4 tetrahedra enframe channels with Pb atoms in the $Pb_2[Ni(PO_4)_2]$ structure (Fig. 7b). One additional vertex of the NiO_6 octahedron compared to the AlO_5 bipyramid provides more complex way of polyhedron connection: one half of PO_4 tetrahedra in the lead nickel phosphate shares oxygen edges with NiO_6 octahedra. Likewise the previous cases channels parallel to the *a* axis of the $Fe^{3+}Fe^{2+}_{0.5}(H_2O)_2(HPO_4)_2$ unit-cell have open 12-memebered windows that are formed by alternating sharing vertices octahedra and tetrahedra (Figure 7c). But in contrast to the $RbCu[Al(PO_4)_2]$ and $Pb_2[Ni(PO_4)_2]$ structures where each AlO_5- or NiO_6-polyhedron belongs to three 12-membered windows, every FeO_6 octahedron is shared between two similar windows in the $(H_2O)_2[Fe_{1.5}(HPO_4)_2]$ crystal structure. Here, the channels along [100] are essentially defined by hydrogen bonds between H_2O molecules, acid phosphate groups and O atoms.[16]

Table 4 Composition, crystal characteristics and selected distances for topologically related phosphates

Formula	Unit-cell parameters *a*, *b*, *c*, Å	Unit-cell angle β, o and *V*, Å^3	Space group, *Z*, ρ, g/cm^3	<M–O>, Å	<P1–O>, Å <P2–O>, Å	Ref.
$RbCu[Al(PO_4)_2]$	5.072(1) 14.070(2) 9.352(1)	100.41(1) 656.4(2)	$P2_1/c$ 4 3.70	1.837 (M=Al^{3+})	1.538 1.532	Our data
$Pb_2[Ni(PO_4)_2]$	5.285(2) 15.464(5) 8.436(3)	90.04(1) 689.4(4)	$P2_1/c$ 4 6.39	2.076 (M=Ni^{2+})	1.546 1.545	15
$(H_2O)_2[Fe_{1.5}(HPO_4)_2]$	5.152(1) 16.629(2) 8.748(1)	90.84(1) 749.5(2)	$P2_1/n$ 4 2.70	2.149 (M1=Fe^{2+}) 1.991 (M2=Fe^{3+})	1.541 1.534	16

The 3*D* framework structures of $RbCu[Al(PO_4)_2]$ and $Pb_2[Ni(PO_4)_2]$ comprise two channels with four-membered windows and two channels with 12-membered windows, for their unit-cells (Figure 8). An additional Fe atom at the center of symmetry in the $(H_2O)_2[Fe_{1.5}(HPO_4)_2]$, provides the structure transformation: it still consists of channels framed by four- and 12-membered windows, but in a different ratio equal to 2:1 (Figure 8c). The large channels differ in apertures that are obviously depending on their content. Thus, a roughly uniform distribution of Pb^{2+} cations leads to more symmetrical windows in the $Pb_2[Ni(PO_4)_2]$ structure with the shortest distance between P1 and P2 positions of 5.28 Å and the largest one between two P1 positions of 12.68 Å. Different in size and charge Rb^+ and Cu^{2+} cations define further distortion of the windows, which have analogous distances of 4.43 and 13.13 Å in the $RbCu[Al(PO_4)_2]$ structure (Figure 7, 8). The stability of the $(H_2O)_2[Fe_{1.5}(HPO_4)_2]$ crystal structure is significantly ensured by short-range hydrogen bonding that has a strong influence on the arrangement of windows with the P2-P2 distance of 4.92 Å and the P1-P1 distance of 11.05 Å (Figure 8).

Physical properties. Thermodynamic properties of $RbCuAl(PO_4)_2$, i.e. specific heat Cp and magnetization M, were studied using relevant options of "Quantum Design" Physical

View Article Online
DOI: 10.1039/C5DT04543F

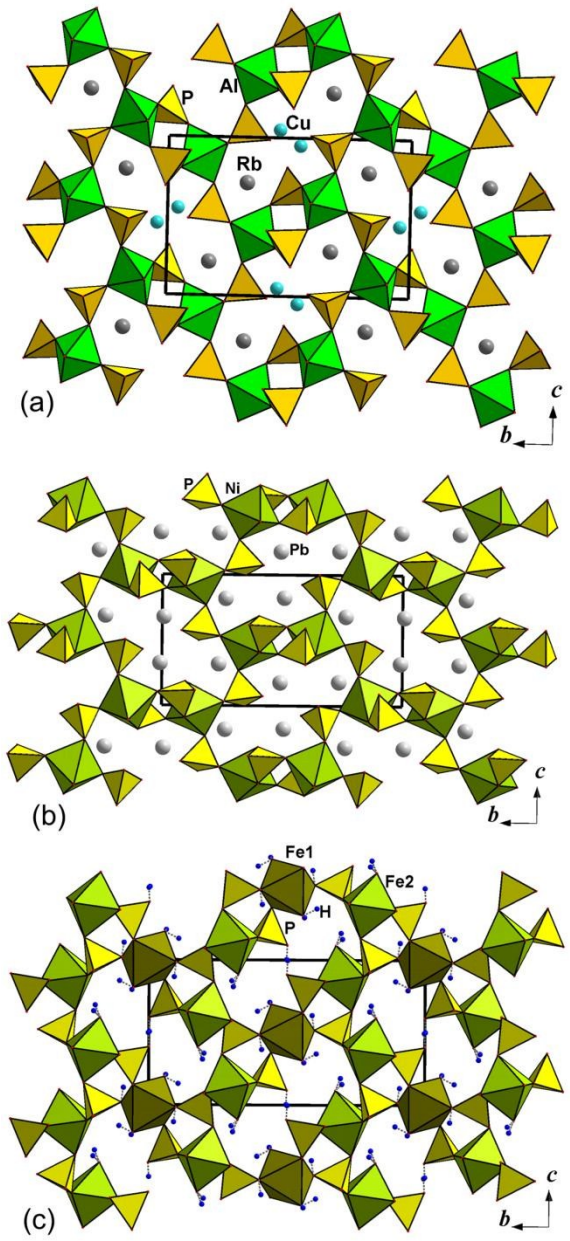

Fig. 7 3*D* frameworks in the $RbCuAl(PO_4)_2$ (*a*), $Pb_2Ni(PO_4)_2$ (*b*) and $Fe^{3+}Fe^{2+}_{0.5}(H_2O)_2(HPO_4)_2$ (*c*) crystal structures in *yz* projections.

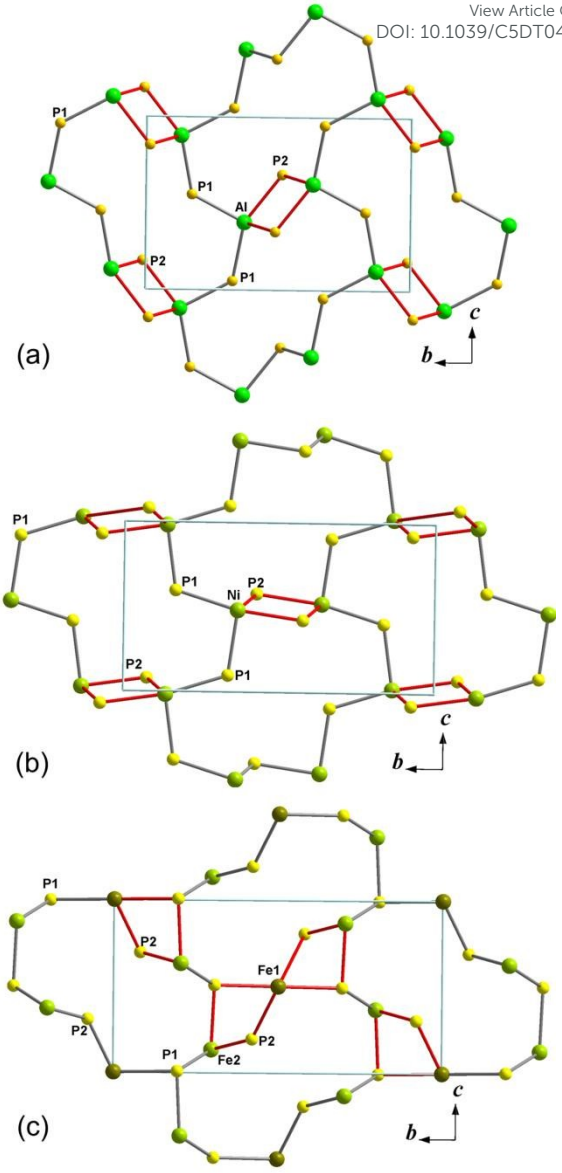

Fig. 8 Topologically similar fragments of cationic substructures in the crystal structures of: a – $RbCuAl(PO_4)_2$, b – $Pb_2Ni(PO_4)_2$, and c – $Fe^{3+}Fe^{2+}_{0.5}(H_2O)_2(HPO_4)_2$

Properties Measurement System PPMS – 9T in the range 2 – 300 K. Electron spin resonance spectrum of $RbCuAl(PO_4)_2$ was measured at room temperature using X-band ESR spectrometer "Adani".

The temperature dependences of magnetic susceptibility χ = M/B of $RbCuAl(PO_4)_2$ taken at both field-cooled (FC) and zero-field-cooled (ZFC) regimes at B = 0.1 T are shown in the upper panel of Fig. 9. At elevated temperatures, the χ(T) dependences follow the Curie-Weiss law with inclusion of temperature-independent term χ_0, i.e. $\chi = \chi_0 + C/(T - \Theta)$, where C is the Curie constant and Θ is the Weiss temperature. The fitting of the FC curve in the temperature range 200 – 300 K gives $\chi_0 = 5.84\times10^{-4}$ emu/mol, C = 0.435 emu K/mol and Θ = 15 K.

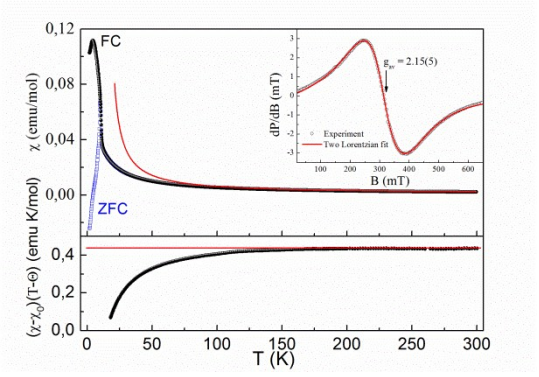

Fig. 9 The temperature dependences of magnetic susceptibility of $RbCuAl(PO_4)_2$ in both FC and ZFC regimes (upper panel), the inset to this panel represents the ESR spectrum of the title compound taken at room temperature. The temperature dependence of the Curie constant is shown in the lower panel.

The temperature independent term is comprised of diamagnetic Pascal and paramagnetic van Vleck contributions. The positive value of χ_0 indicates the predominance of van Vleck term χ_{para} = 7.18×10^{-4} over the sum of the Pascal constants of individual ions χ_{dia} = - 1.34×10^{-4} emu/mol.[17] The van Vleck contribution is defined by the splitting of Cu^{2+} ions d-shell in distorted octahedral environment. The positive value of the Weiss temperature Θ points to prevailing role of ferromagnetic exchange interactions at high temperatures. At lowering temperature, the experimental data strongly deviate from the extrapolation of the fitting curve shown by solid line in the upper panel of Fig. 9. It means the strengthening of antiferromagnetic exchange contribution. That same is seen in the temperature dependence of the Curie constant C shown in the lower panel of Fig. 9. The value of C defined in the range 200 – 300 K gives effective magnetic moment of Cu^{2+} ions μ_{eff} = 1.87 μ_B. This value exceeds free electron value 1.73 μ_B, but is in very good correspondence with numerical estimation assuming the g-factor of Cu^{2+} ions g = 2.155 as found in the electron spin resonance measurements (see the Inset to upper panel of Fig. 9).

The FC and ZFC magnetization curves sharply split below T_N = 10.5 K. The magnetization continues raise below T_N when measured in FC regime and drops to negative values when measured in ZFC regime. The latter circumstance could be due to small negative frozen magnetic field of superconducting solenoid of PPMS – 9T device. The overall behavior of magnetization of $RbCuAl(PO_4)_2$ in magnetically ordered state suggests the presence of weak spontaneous magnetic moment and formation of ferromagnetic domain structure. At low magnetic field, the response of this structure to the temperature variation leads to the Schottky-type anomalies in both magnetization and specific heat.

In fact, the findings of magnetization study are fully corroborated by specific heat measurements. The temperature dependence of specific heat Cp is shown in Fig. 10. Firstly, it shows absence of any structural transformations in $RbCuAl(PO_4)_2$ below room temperature. At T_N = 10.5 K, the specific heat evidences rather modest peak associated with the long-range magnetic ordering in the system. The peak's magnitude is heavily suppressed due to the fact that the main part of magnetic entropy is released well above the Neel temperature as follows from the temperature dependence of the Curie constant C. The much stronger anomaly in low temperature specific heat at T_{max} ~ 3.5 K is associated tentatively with temperature assisted dynamics of ferromagnetic domains. The overall behavior of Cp at $T < T_N$ can be represented by the sum of Schottky-type and cubic terms, as shown in the lower Inset to Fig. 10.

Finally, let us discuss the origin of ferromagnetic-type response in $RbCuAl(PO_4)_2$. The magnetic subsystem in this compound is represented by chains of CuO_6 octahedra coupled by interchain interactions through PO_4 and AlO_5 polyhedra. Within the chains the CuO_6 octahedra are coupled alternatively through the *cis*- and *trans*- edges. The same crystallographic motif is found in pyroxenes.[18,19] Such

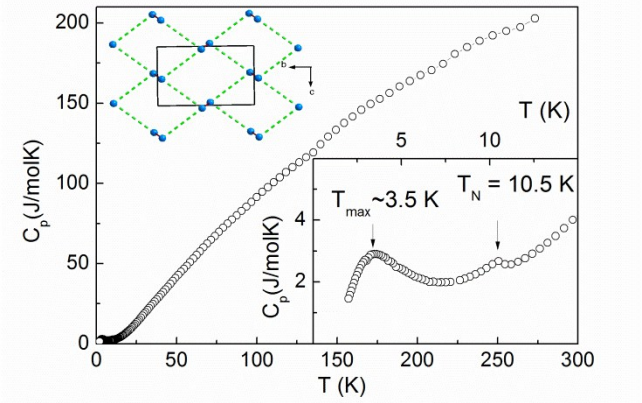

Fig. 10 The temperature dependence of specific heat of $RbCuAl(PO_4)_2$. The lower inset represents enlarged low temperature region. The upper inset shows the topology of Cu^{2+} subsystem in the title compound.

arrangement of magnetic centers presumes strong alternation of intrachain exchange interaction parameters. The Cu – O – Cu angle for *trans*- sharing units is ~ 80°, while that for *cis*- sharing units is ~ 97°. It allows presuming that ferromagnetic and antiferromagnetic exchange interactions alternate within the chains. Moreover, ferromagnetic intrachain interaction seemingly prevails taking into account the positive value of the Weiss temperature. The interchain exchange interaction is antiferromagnetic which follows from the deviation of experimental data from the fitting curve at lowering temperature. Therefore, the overall magnetic order is mainly of antiferromagnetic nature. However, the magnetic response of $RbCuAl(PO_4)_2$ at $T < T_N$ suggests weak ferromagnetism which arises tentatively due to the canting of otherwise antiparallel magnetic moments of Cu^{2+} ions. The canting is the sequence of antisymmetric exchange between two moments coupled by Dzyaloshinskii – Moriya interaction.[20,21] As shown in the upper Inset to Fig. 10, this type of interaction could be present for interchain exchange pathways shown in the upper Inset to Fig. 10 by dashed lines.

Conclusions

The rubidium copper aluminum phosphate $RbCuAl(PO_4)_2$ has been hydrothermally synthesized at 553 K. The new monoclinic phase crystallizes in a structure type lately established for three isotypic iron phosphates $KMFe(PO_4)_2$ with *M* = Fe/Ni, Ni, Mg or Co. The topological similarities between microporous $RbCuAl(PO_4)_2$, $Pb_2Ni(PO_4)_2$ and $Fe^{3+}Fe^{2+}_{0.5}(H_2O)_2(HPO_4)_2$ crystal structures have been revealed in a course of our study. The title compound orders antiferromagnetically at T_N = 10.5 K and exhibits spontaneous magnetization in magnetically ordered state.

Acknowledgements

We thank O.V. Yapaskurt for the X-Ray spectral analysis of the sample and N.V. Zubkova for the help in the X-Ray experiment.

View Article Online
DOI: 10.1039/C5DT04543F

This work was supported in part from the Ministry of Education and Science of the Russian Federation in the framework of Increase Competitiveness Program of NUST «MISiS» (№ К2-2015-075) and by RFBR projects 15-05-06742, 14-02-00111 and 14-02-00245.

Notes and references

‡ The analysis was performed at the Laboratory of Local Methods for Studying Materials, Department of Petrology, Faculty of Geology, M.V. Lomonosov Moscow State University.

§ Additional materials to the crystal structure investigation are obtained from Fachinformationszentrum Karlsruhe, Germany, under specification of deposit No. CSD-429837 and authors reference.

1 A. K. Cheetham, G. Férey, T. Loiseau, *Angew. Chem.* 1999, **111**, 3466.
2 D. Maspoch, D. Ruiz-Molina, J. Veciana, *Chem. Soc. Rev.* 2007, **36**, 770.
3 J. A. Armstrong, E. R. Williams, M. T. Weller, *J. Am. Chem. Soc.* 2011, **133**, 8252.
4 M. S. Whittingham, *Chem. Rev.* 2014, **114**, 11414.
5 E. R. Williams, S. A. Morris, M. T. Weller, *Dalton trans.* 2012, **41**, 10845.
6 S. Natarajan, S. Mandal, *Angew. Chem. Int. Ed.* 2008, **47**, 4798.
7 L. J. Farrugia, *J. Appl. Crystallogr.* 2012, **45**, 849.
8 *International Tables for Crystallography*, ed. E. Prince, Kluwer, Dordrecht, 3rd Edn., 2004, Tables 4.2.6.8 and 6.1.14.
9 A. Altomare, G. Cascarano, C. Giacovazzo, A. Guagliardi, M. C. Burla, G. Polidori, M. Camalli, *J. Appl. Crystallogr.* 1994, **27**, 435.
10 G. M. Sheldrick, *Acta Crystallogr*. 2008, **A64**, 112.
11 I. D. Brown, D. Altermatt, *Acta Crystallogr.* 1985, **B41**, 244.
12 I. D. Brown, *Chem. Rev.* 2009, **109**, 6858.
13 N. Yu. Strutynska, I. V. Zatovsky, V. N. Baumer et._al., *Acta Crystallogr.* 2014, **C70**, 160.
14 M. Badri, A. Hidouri, M. L. Lopez, M. L. Veiga, C. Pico, J. Darriet, M. Ben Amara, *J. Struct. Chem.* 2015, **56**, 714.
15 Zh. He, W. Zhang, T. Xia, W. Yu, W. Cheng, *Dalton Trans.* 2013, **42**, 5480.
16 I. Vencato, Y. P. Mascarenhas, E. Mattievich, *Am. Mineral*. 1986, **71**, 222.
17 G. A. B ain, J. F. Berry, *J. Chem. Educ*. 2005, **85**, 532.
18 A. N. Vasil'ev, T.N. Voloshok, O. L. Ignatchik, M. Isobe, Y. Ueda, JETP Lett. 2002, **76**, 35.
19 M. Isobe, E. Ninomiya, A. N. Vasil'ev, Y. Ueda, *J. Phys. Soc. Jpn.* 2002, **71**, 1423.
20 I. Dzyaloshinskii, *J. Phys. Chem. Solids.* 1958, **4**, 241.
21 T. Moriya, *Phys. Rev*. 1960, **120**, 91.